Scientia Iranica B (2017) 24(5), 2396–2405

SCIENTIA IRANICA

Sharif University of Technology
Scientia Iranica
Transactions B: Mechanical Engineering
www.scientiairanica.com

Piezoelectric energy harvesting from vertical piezoelectric beams in the horizontal fluid flows

Y. Amini[a,*], H. Emdad[b] and M. Farid[b]

a. *School of Mechanical Engineering, PG University, Boushehr, Iran.*
b. *School of Mechanical Engineering, Shiraz University, Shiraz, Iran.*

Received 24 October 2015; received in revised form 27 July 2016; accepted 21 August 2016

KEYWORDS
Energy harvesting;
Piezoelectric;
Gurney flap;
Vortex shedding;
Fluid-structure interaction;
Aero-elasticity.

Abstract. Piezoelectric Energy Harvesting (PEH) of fluid-flow energy has attracted significant attention throughout the last decade. In the previous PEH from fluid flow, a piezoelectric beam was placed behind a bluff body, such as circular cylinders. Hence, the piezoelectric beam oscillated due to the vortex shedding behind of the bluff body. Subsequently, this vibration generated voltage in the beam. In many engineering vehicles such as airplanes, the strong vortex shedding caused by bluff body was destructive and reduced the efficiency of devices; therefore; it was not proper to attach a bluff body to these devices. In this paper, PEH from vertical beams in low speeds and high-speed flows is investigated. The current work shows that in contrast to low-speed flows, the extracted power from vertical beam in high-speed flows is considerable. Moreover, as a practical example of vertical beam in high-speed flows, the energy harvesting from piezoelectric Gurney flap attached to an NACA2412 airfoil is investigated. Finally, this study proposes a piezoelectric vertical beam with attached end cylinder as an energy harvester in the low-speed flows. It is indicated that this device has strong vibration and, therefore, produces a remarkable electrical power.

1. Introduction

Portable electronics and wireless technology have several advantages compared to the traditional wired devices, including ability to be placed anywhere, smallness, neatness (no untidy cables), and low power consumption. Consequently, Wireless Sensor Networks (WSNs) technology has gained increasing attention in industrial automation [1-4], structural health monitoring [5-9], agriculture [7], and military applications [10-13]. Although the electrochemical batteries are usual power sources for these sensors, energy harvesting has some advantages compared to them and has attracted significant attention throughout the last decade. Energy Harvesting (EH) is the process of extracting unused energy from the ambient environment in the vicinity of the sensors and converting it into a usable form of electrical energy. EH can use various energy sources such as solar energy, thermal energy, wind energy, vibrational energy, and kinetic energy. Mechanical vibrations are found almost everywhere, in the running automobiles and airplanes, rotating machines, buildings and bridges, air ducts, railways, industrial plant equipment, and people's walking or breathing. Therefore, the mechanical vibrations are one of the

*. *Corresponding author.*
E-mail addresses: aminiyasser@pgu.ac.ir (Y. Amini); hemdad@shirazu.ac.ir (H. Emdad); farid@shirazu.ac.ir (M. Farid)

doi: 10.24200/sci.2017.4240

most important sources for EH. The mechanical vibration energy can be converted to electrical energy by using electromagnetic [14-16], piezoelectric [17-19], and electrostatic [20-22] mechanisms. The piezoelectric transduction has some advantages such as high power density, very simple design, and very small size [23-26] in comparison with other alternatives. Moreover, unlike the electrostatic transduction, it does not require bias voltage input. Normally, a piezoelectric energy harvester is a thin cantilevered beam with one (unimorph) or two (bimorph) piezoelectric layers.

A Single-Degree-Of-Freedom model (SDOF) is the simplest mathematical model which has been used for numerical simulation of piezoelectric energy harvesters [27,28]. In this approach, the beam is modeled by a second-order ordinary differential equation with the beam tip displacement as its dependent variable. Although the SDOF modeling can be easily solved by giving an initial comprehension into the problem, it is only a simple approximation restricted to a single vibration mode of the beam and it cannot predict some significant features of the physical behavior of the harvester. Recently, Erturk and Inman [29] showed that for harmonic base excitation, the SDOF model might yield highly inaccurate results for transverse vibrations of cantilevered beams as well as longitudinal vibrations of bars. For increasing the accuracy of the solution, Sodano et al. [25] and duToit et al. [26] employed the Rayleigh-Ritz method [30] for modeling of cantilevered piezoelectric energy harvesters. Furthermore, the analytical solutions for constant cross section and material properties for harmonic base excitation were given by Erturk and Inman [18,31]. Amini et al. [32] presented a finite element modeling for functionally graded piezoelectric harvesters. Recent interests in piezoelectric energy harvesting from fluid flow energy have prompted new developments of energy generators. Some of these works are reviewed in the following. Since Unmanned Air Vehicles (UAVs) have limited energy during their operations, they can be considered as a practical application for energy harvesting [33]. The mechanical vibration due to unsteady aerodynamic loads is one of the available sources for piezoelectric energy harvesting in UAVs [33]. Furthermore, air flow has a high energy density and it is another candidate for PEH in these vehicles and for PEH from wind. In these cases, a Fluid Structure Interaction (FSI) problem occurs and a small part of the fluid flow momentum is converted to the vibrational energy in piezoelectric beam and, then, this energy is transformed to the electrical energy by piezoelectric effect. Allen and Smits [34] studied the behavior of long and very flexible piezoelectric strips (so-called 'eels') in the wake of a flat plate normal to a flow, experimentally. Taylor et al. [35] fabricated an eel structure of piezoelectric polymer to convert mechanical flow energy to electrical power. Tang et al. [36] designed a flutter-mill to generate electricity by extracting energy from fluid flow. Their structure was similar to the eel systems of Allen and Smits [34] and Taylor et al. [35]. They investigated the energy transfer between the structure and the fluid flow through an analytical approach. These authors utilized the flow induced vibrations of fluid-structure interaction system to extract energy from the surrounding fluid flow. Generally, PEH from fluid flows is a triple coupling among the fluid flow, the piezoelectric material, and the electronic circuit. Thus, its numerical simulation should contain some solver for solving the governing equations of fluid flow, piezoelectric material, and electric circuit. Akaydın et al. [37,38] placed a piezoelectric beam in the wake of a circular cylinder for energy harvesting from fluid flow. They used FLUENT software to simulate the three-way interactions of the turbulent flow, piezoelectric structure, and the harvester electronic circuit. They developed a User-Defined Function (UDF) based on the SDOF model to simulate the piezoelectric beam. In this modeling, for simplicity of electro-mechanical coupling, the open circuit condition ($R = \infty$) was assumed. In open circuit condition, both governing equations of piezoelectric structure and electrical circuit are reduced to a second-order ordinary differential equation. As mentioned earlier, the SDOF model has not sufficient accuracy for modeling of piezoelectric energy harvester. Amini et al. [39] developed and validated an accurate modeling for simulation of interaction among turbulent flow, piezoelectric structure, and electronic circuit. In this model, the piezoelectric structure was simulated by the Finite Element Method (FEM). Moreover, this model was not limited to open-circuit condition and any value of Resistance (R) could be used in the simulation.

In this study, energy harvesting from vertical piezoelectric beams in the horizontal flows is investigated by the accurate model proposed by Amini et al. [39]. To this purpose, vertical piezoelectric beams for various inlet flow speeds are investigated. The results show that in high-speed flows such as flow around airfoils, the vertical beam has sufficient vibration to produce considerable electrical power. Moreover, in such cases, the vertical beam behaves similar to the Gurney flap, which improves the aerodynamics of wings by increasing the lift with only small change in the drag penalties. In the low-speed flows, the vertical beam has not sufficient vibration and, therefore, the extracted power is not remarkable. This study shows that in the low-speed flows, the vertical beam with attached end cylinder has strong vibration and, therefore, produces a remarkable electrical power. It should be noted that in this study, the code of Amini et al. [39] is used. The code is validated by experimental results in that work.

2. Governing equations and solution methodology

2.1. Finite element modeling of a piezoelectric beam energy harvester

By using the semi-discrete Finite Element (FE) formulation and employing the cubic Hermitian shape functions, the following system of ordinary differential equations is obtained for each element [39]:

$$\begin{cases} M_{ij}^e \ddot{U}_j^e + C_{ij}^e \dot{U}_j^e + K_{ij}^e U_j^e - \theta_i^e \nu = F_i^e & \text{(1a)} \\ C_p \frac{dv}{dt} + \frac{\nu}{R} + \theta_i^e \dot{U}_i^e = 0 & \text{(1b)} \end{cases}$$

where:

$$M_{ij}^e = \left(\int_0^L \left[(\rho_s I_s + \rho_p I_p) \frac{\partial \psi_i}{\partial x} \frac{\partial \psi_j}{\partial x} + (\rho_s A_s + \rho_p A_p) \psi_i \psi_j \right] dx \right), \quad (2)$$

$$K_{ij}^e = \int_0^L \left(Y_s I_s + c_{11}^E I_p \right) \frac{\partial^2 \psi_i}{\partial x^2} \frac{\partial^2 \psi_j}{\partial x^2} dx, \quad (3)$$

$$F_i^e = \int_0^L \psi_i q(x) dx. \quad (4)$$

The damping matrix $\mathbf{C}$ in Eq. (1a) is often taken to be a linear combination of the mass and stiffness matrices (Rayleigh damping), $\mathbf{C} = \alpha \mathbf{M} + \beta \mathbf{K}$, where α and β are determined in physical experiments. In Eq. (1b), θ_i^e and C_p can be obtained as:

For unimorph configuration:

$$\theta_i^e = \frac{\beta_p e_{31}}{h_p} \frac{\partial \psi_i}{\partial x} \Big]_0^l, \qquad C_p = \frac{b \varepsilon_{33} L}{h_p}.$$

For bimorph with series configuration:

$$\theta_i^e = \frac{\beta_p e_{31}}{2h_p} \frac{\partial \psi_i}{\partial x} \Big]_0^l = \frac{b e_{31} (h_p + h_s)}{2},$$

$$C_p = \frac{b \varepsilon_{33} L}{2h_p}.$$

For bimorph with parallel configuration:

$$\theta_i^e = \frac{\beta_p e_{31}}{h_p} \frac{\partial \psi_i}{\partial x} \Big]_0^l = b e_{31} (h_p + h_s),$$

$$C_p = \frac{2b \varepsilon_{33} L}{h_p}.$$

In the present study, Newmark family of time-approximation schemes is used to approximate the second-order time derivatives to convert the differential equations to algebraic ones. In this approximation, in the $(s+1)$th time step, the nodal deflections and slopes can be obtained by solving the following system of algebraic equations [39]:

$$\hat{\mathbf{K}}^{s+1} \mathbf{U}^{s+1} = \hat{\mathbf{F}} + \mathbf{\Theta}^{s+1} \boldsymbol{\nu}^{s+1}, \quad (5)$$

in which:

$$\hat{\mathbf{K}}^{s+1} = \mathbf{K}^{s+1} + a_3 \mathbf{M}^{s+1} + a_6 \mathbf{C}^{s+1}, \quad (6)$$

$$\hat{\mathbf{F}} = \mathbf{F}^{s+1} + \mathbf{M}^{s+1} \mathbf{A}^s + \mathbf{C}^{s+1} \mathbf{B}^s, \quad (7)$$

$$\mathbf{A}^s = a_3 \left(\mathbf{U}^s + \Delta t \dot{\mathbf{U}}^s + \frac{1}{2} (1-\gamma) \Delta t^2 \ddot{\mathbf{U}}^s \right), \quad (8)$$

$$\mathbf{B}^s = a_6 \mathbf{U}^s + a_7 \dot{\mathbf{U}}^s + a_8 \ddot{\mathbf{U}}^s, \quad (9)$$

$$a_1 = \alpha \Delta t, \qquad a_2 = (1-\alpha),$$

$$a_3 = \frac{1}{\beta \Delta t^2}, \qquad a_4 = \frac{1}{\beta \Delta t}, \qquad a_5 = \frac{1}{\gamma} - 1. \quad (10)$$

After solving the algebraic system (Eq. (5)), new nodal velocities and accelerations are calculated as:

$$\ddot{\mathbf{U}}^{s+1} = a_3 \left(\mathbf{U}^{s+1} - \mathbf{U}^s \right) - a_4 \dot{\mathbf{U}}^s - a_5 \ddot{\mathbf{U}}^s, \quad (11)$$

$$\dot{\mathbf{U}}^{s+1} = \dot{\mathbf{U}}^s + a_2 \ddot{\mathbf{U}}^s + a_1 \ddot{\mathbf{U}}^{s+1}. \quad (12)$$

Finally, the average electrical power generated between times t_0 and t_1 can be calculated as:

$$P_{\text{elec}} = \frac{1}{R(t_1 - t_0)} \int_{t_0}^{t_1} \nu^2 dt. \quad (13)$$

2.2. Governing equation of fluid flow with dynamic mesh motion

The governing equations of the fluid flow are the incompressible Reynolds Averaged Navier-Stokes ones (RANS). Since a moving boundary exists in the fluid domain, Arbitrary Lagrangian Eulerian (ALE) formulation is used. The RANS equations on a moving mesh should be used in the following forms [40,41]:

$$\nabla \cdot \boldsymbol{\nu} = 0,$$

$$\rho \frac{\partial \boldsymbol{\nu}}{\partial t} + \rho (\boldsymbol{\nu} - \hat{\boldsymbol{\nu}}) \cdot \nabla \boldsymbol{\nu} = -\nabla p + \nabla \cdot \left((\mu + \mu_t) \nabla \boldsymbol{\nu} \right),$$

$$\hat{\boldsymbol{\nu}} = \frac{d \hat{\mathbf{u}}}{dt}, \quad (14)$$

where ρ, $\boldsymbol{\nu}$, p, μ, and t are the density, the average velocity, the average pressure, the viscosity, and the

time, respectively. $\hat{\nu}$ and $\hat{\mathbf{u}}$ represent the velocity and the displacement of the mesh nodes, respectively. μ_t is the turbulent viscosity, which can be predicted by $k-\omega$SST [42] turbulent model based on the Boussinesq approximation.

At the interface of the fluid and structure domains, interaction is considered by transferring the fluid flow stress to the structure and the structural displacements to the fluid flow. Also, it is assumed that the fluid always remains in contact with the structure. Therefore, compatibility on the displacement and no-slip condition requires that:

$$\mathbf{T}^s \cdot \mathbf{n} = \mathbf{T}^F \cdot \mathbf{n},$$

$$\mathbf{u}^s = \mathbf{u}^F, \tag{15}$$

where $\mathbf{n}$, $\mathbf{T}$, and $\mathbf{u}$ are the unit normal boundary vector, the stress tensor, and the displacement, respectively. In the ALE approach, the fluid internal mesh should be deformed in response to the fluid structure interface displacements. However, the deformation of fluid mesh is unknown and it should be found in terms of the structural deformation. In the present work, the Laplacian operator is used for the dynamic mesh motion in the fluid mesh. In this method the mesh vertices displacement, $\hat{\mathbf{u}}$, is computed by solving the Laplacian equation in the following form [43,44]:

$$\nabla \cdot (\gamma \nabla \hat{\mathbf{u}}) = 0, \tag{16}$$

where γ is the diffusion coefficient. The boundary condition for this equation is:

$$\hat{\mathbf{u}} = \begin{cases} \mathbf{u}^s & \text{for fluid solid interface boundary} \\ 0 & \text{for other boundaries} \end{cases} \tag{17}$$

3. Numerical results

3.1. Energy harvesting from vertical piezoelectric beams in horizontal flow

In this section, energy harvesting from vibrations of unimorph vertical beam in a horizontal fluid flow is investigated. The schematic drawing of vertical beam and fluid flow is shown in Figure 1.

The advantage of vertical beam for energy harvesting in comparison with horizontal beam in the wake of cylinder is that it can be simply attached to a wall and does not need the upstream cylinder or blunt body. In the following, energy harvesting by different inlet velocities and beam stiffnesses is examined. In this study, the height of beam is assumed to be 10 cm, the thicknesses of piezoelectric layer and substructure layer are assumed to be 0.1 mm and 0.7 mm, and the value of load resistance in all simulations of vertical unimorph beam is supposed to be $R = 10$ MΩ. The properties of this unimorph piezoelectric beam are given in Table 1.

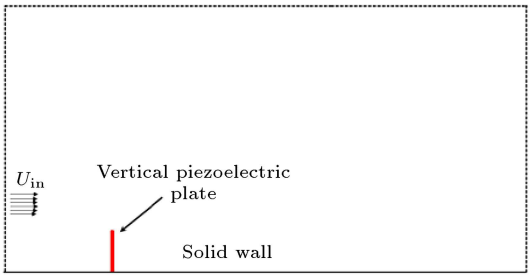

Figure 1. Schematic drawing of a vertical flexible beam in the horizontal fluid flow.

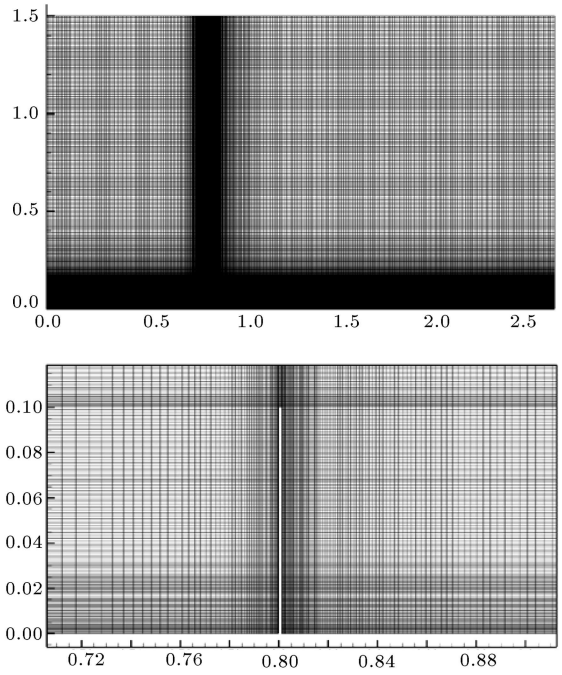

Figure 2. Structured mesh and its detailed view around the vertical flexible beams.

The numerical grid for vertical piezoelectric beam harvester is shown in Figure 2. This grid has 120,000 elements and for capturing boundary layer and accuracy of $k-\omega$SST turbulent model, the elements are refined near the wall so that the y^+ on the wall is less than 1. It is worth noting that the capacitance property of the piezoelectric materials prevents the DC current caused by static deformation. Therefore, the produced voltage of piezoelectric materials oscillates around the value of zero. In contrast with horizontal beam in the wake of cylinder, the static (average) deformation in vertical beams has nonzero value. Since, in the SDOF used by Akaydin et al. [38], the voltage is proportional to the displacement, this model predicts a nonzero value for the predicted average voltage, which is completely wrong. Hence, the SDOF model of Akaydin et al. [38] cannot be used in numerical simulation of energy harvesting from vertical beams and, for these harvesters, the accurate algorithm should be used.

Figures 3 and 4 show the time history of beam

Table 1. Geometric and material properties of the unimorph vertical harvester.

Young's modulus of the piezoelectric	Y_p (GPa)	3
Mass density of the substructure	ρ_s (kg/m^3)	1390
Mass density of the piezoelectric	ρ_p (kg/m^3)	1780
Effective piezoelectric stress constant	e_{31} (C/m^2)	0.07
Permittivity	ε_{33}^s (nF/m)	0.08
Proportional constant	α (rad/s)	4.886
Proportional constant	β (s/rad)	1.2433×10^{-5}

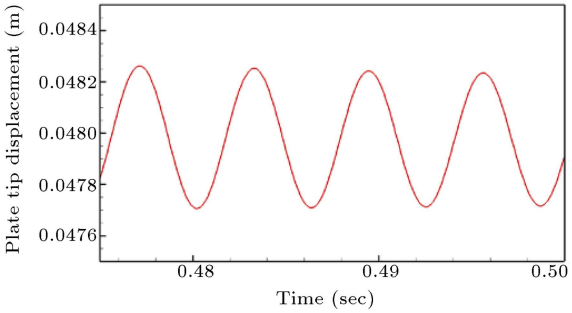

Figure 3. Time history of the beam tip displacement (m) for $R = 10$ MΩ.

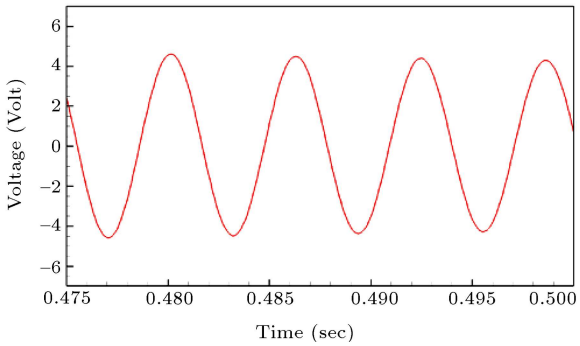

Figure 4. Time history of the produced voltage (Volt) for $R = 10$ MΩ.

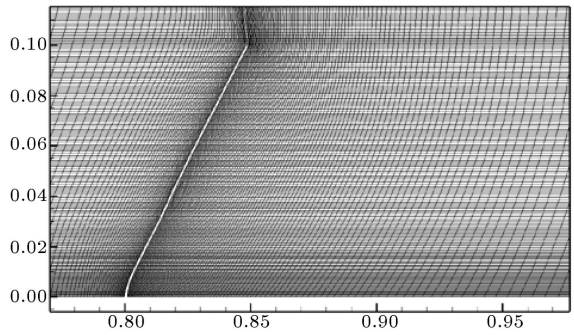

Figure 5. Maximum deformed shape of vertical flexible beam.

Table 2. Extracted power (μW) for different beam stiffnesses and inlet flow velocities.

		EI (pa.m^4)		
		$EI = 0.005$	$EI = 0.01$	$EI = 0.02$
U_{in} (m/sec)	$U_{in} < 6$	0.0	0.0	0.0
	10	0.04	0.001	0.0
	20	0.4	0.1	0.0
	30	1.05	0.32	0.08
	40	2.5	0.74	0.49
	50	3.6	1.4	0.67

tip displacement and produced voltage for inlet velocity of 40 m/sec and total beam stiffness equal to 0.005 pa.m^4. As can be seen in these figures, the static deflection (average deflection) of beam is 4.8 cm and the amplitude of oscillation around the static deflection is 3 mm. Moreover, these periodic oscillations are caused by vortex shedding effect behind the plate. Furthermore, the voltage oscillates between +5 to −5 volts with average of zero volt. Therefore, the Amini et al. [39] model simulates the capacitance property of piezoelectric materials correctly.

The maximum deformed shape of the beam for $U_{in} = 40$ m/sec and $EI = 0.005$ pa.m^4 is shown in Figure 5. This figure shows that the dynamic mesh solver of the current code can simulate the large deformation without destroying the grid elements.

The harvested power for different beam stiffnesses and inlet flow velocities is cited in Table 2. This table reveals that by increasing the inlet velocity, the harvested power increases. Moreover, when the inlet velocities are lower than 6 m/sec, the oscillations of beam and, subsequently, the extracted power are negligible. For generating considerable power, the inlet velocity should be greater than 30 m/sec. Therefore, only in the high-speed vehicles such as aerospace ones the vertical beam can be used as piezoelectric energy harvester. In the following section, a vertical beam is considered as piezoelectric Gurney flap and used for energy harvesting.

3.2. Energy harvesting from piezoelectric Gurney flap

The Gurney flap is a vertical short flap mounted perpendicular to the pressure side of the airfoil surfaces. The size of a Gurney flap usually ranges from 1 to 5 percent of chord. It can have relatively powerful effect

on the aerodynamics of a wing, increasing lift with only small change of drag penalties. Moreover, the high bandwidth and good control authority make the device an ideal candidate for control of flight vehicle. Since bluff bodies produce a huge vortex shedding and, consequently, reduce the efficiency of aerospace vehicles, it is not good to attach a bluff body to such devices. Accordingly, for aerospace vehicles, the energy harvester should not damage its aerodynamics performance. To this purpose, in the present study, an airfoil with piezoelectric Gurney flap is considered. By using a piezoelectric Gurney flap, not only the aerodynamics of airfoils are improved, but also the electrical energy required for the sensors placed on the airfoil is extracted. In this section, a piezoelectric Gurney flap is attached to an NACA2412 airfoil and the power generation by Gurney flap oscillation is investigated. The free stream Mach number is 0.3 and the angles of attack are equal to 2°. The length, thickness (h) and depth (b) of piezoelectric Gurney flap used in the present investigation are 40 mm, 1 mm, and 16 mm, respectively. The Gurney flap is composed of piezoelectric polyvinylidene fluoride (PVDF) layers and a structure with thicknesses $h_p = 28$ μm and $h_s = 972$ μm, respectively. The physical properties of piezoelectric Gurney flap are listed in Table 1.

A high-quality structure mesh is generated and the mesh is refined adjacent to the beam and airfoil so that $y+$ is less than one; also, there exist at least 10 nodes in boundary layer. This mesh is shown in Figure 6.

Figure 7 illustrates the tip displacement of flap for

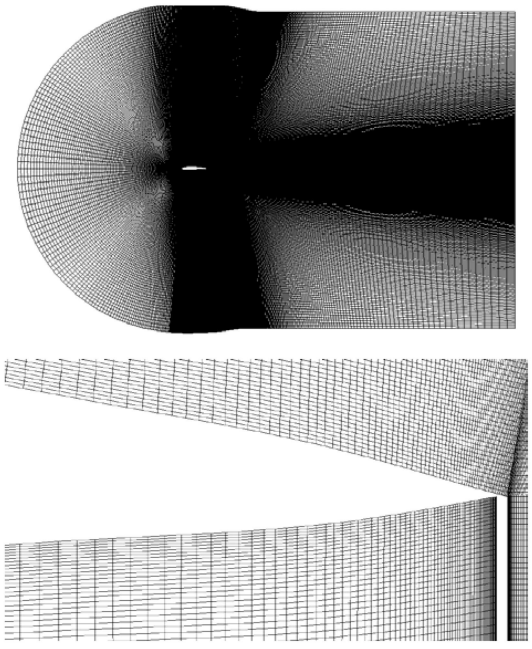

Figure 6. Computational grid for the airfoil and the Gurney flap.

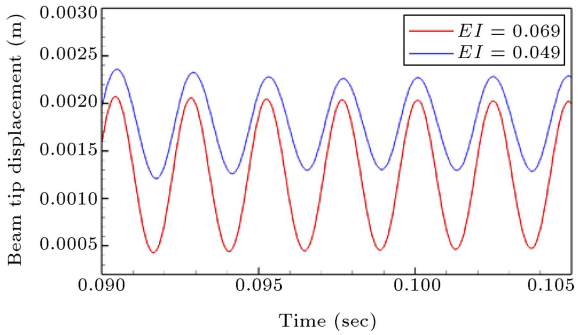

Figure 7. Time history of the Gurney flap tip displacement for $R = 10$ MΩ.

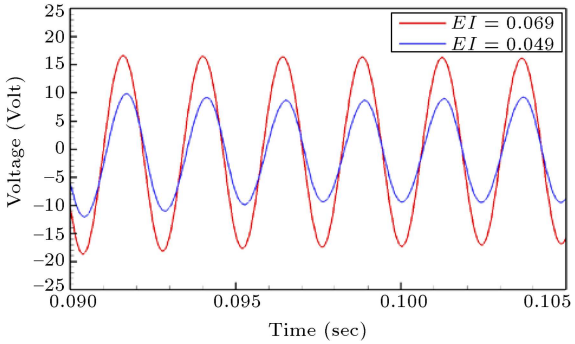

Figure 8. Time history of the produced voltage for $R = 10$ MΩ.

$EI = 0.049$ Pa.m^4 and $EI = 0.069$ Pa.m^4 versus time for angle of attack equal to 2°. As can be seen, the vibration of flap involves a periodic oscillation. Since every periodic vibration is produced by a periodic force, there should be a periodic force on the flap. This periodic force is created by a small vortex behind the Gurney flap. As shown in Figure 7, the amplitude of vibration related to smaller stiffness has smaller values and larger average. However, both stiffnesses have approximately the same frequency of vibrations, which is equal to 454.54 Hz. The voltage related to deflections of this beam is shown in Figure 8. This figure indicates that the voltage amplitudes of smaller and larger stiffnesses are 11 and 19 Volts, respectively. Moreover, the voltage averages of both stifnesses are zero. This zero value for average voltage is related to the capacitance property of the piezoelectric materials.

Using Eq. (13), the calculated power generations are 17.3 μW for $EI = 0.069$ Pa.m^4 and 7 μW for $EI = 0.049$ Pa.m^4. Figure 9 illustrates the pressure contours for $EI = 0.069$ Pa.m^4 at times 0.099 and 0.1 sec. The small vortex, which causes the periodic force on the Gurney flap, can be observed in this figure.

For studying the effects of this vertical beam on the lift and drag coefficients, a three-dimensional (3-D) modeling of airfoil with attached Gurney flap is simulated. The length, thickness, and depth of the

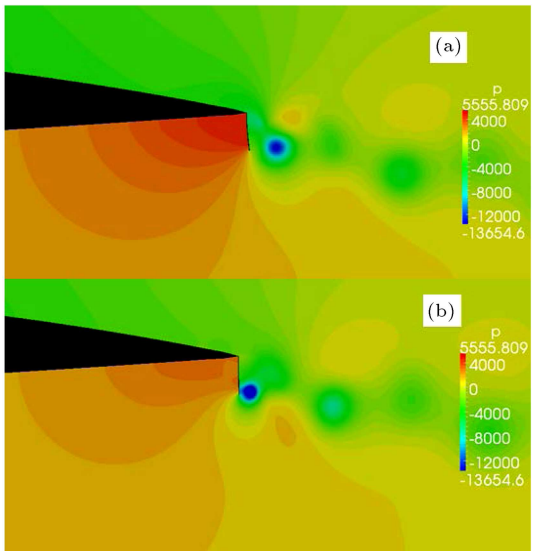

Figure 9. Pressure contour around the Gurney flap for angle of attack equal to 2° at (a) 0.099 sec and (b) 0.1 sec.

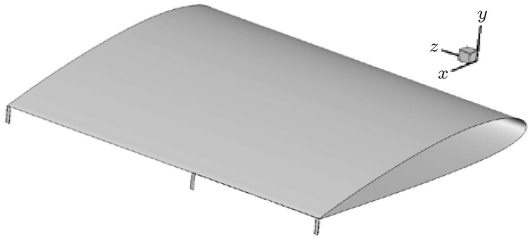

Figure 10. Geometry of 3-D airfoil with vertical plate.

Gurney flap used in this 3-D simulation are 40, 1, and 16 millimeters, respectively. The geometry of this 3-D airfoil with attached gurney flap is shown in Figure 10.

Table 3 contains the lift and drag coefficients of NACA 2412 airfoil with different numbers of vertical beams per each meter of airfoil span. This table reveals that when the number of vertical beams per unit length of span is smaller than two, the effects of vertical beams on the lift and drag coefficients are negligible. But, by increasing the number of vertical beams, both lift and drag coefficients increase. However, the increase in the lift coefficient is larger than that in drag coefficient, leading to increase in lift over drag coefficient.

3.3. Energy harvesting from vertical beams with end cylinder in horizontal flow

As mentioned earlier, vertical piezoelectric beams can be used in high-speed flows for energy harvesting. At low-speed flows, the vertical beam has small vibrations and, therefore, cannot produce considerable power. In this work, a modified shape of the vertical beam is proposed for energy harvesting at low-speed flows. The proposed shape includes a blunt body, such as circular or square cylinder, attached to the tip of the vertical beam. The schematic drawing of this modified shape is shown in Figure 11.

The attached circular or square cylinder produces oscillating forces and moments on the beam, intensifying the piezoelectric beam vibration and, subsequently, increasing the produced voltage and extracted power. For the case study, a harvester comprising a circular cylinder with 2 cm of diameter and a vertical beam of height 10 cm is investigated. For numerical simulation of this harvester, different inlet velocities and stiffnesses are assumed. Details of these simulations and harvested power from them are given in Table 4. In all of these simulations, the piezoelectric constants and properties are the same as cited in Table 1. The numerical grid used for simulations of this harvester involves 132,000 cells displayed in Figure 12.

It is worth noting that in the numerical simula-

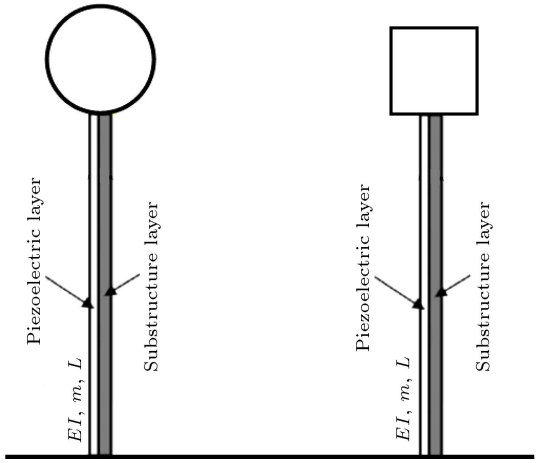

Figure 11. Schematic drawing of a vertical flexible beam with attached cylinder in the horizontal fluid flow.

Table 3. Lift and drag coefficients of 3-D airfoil with different numbers of vertical beams.

Numbers of vertical beam per unit length of span	Lift coefficient (L)	Drag coefficient (D)	Lift over drag coefficient (L/D)
0 (clean airfoil)	0.231	0.0075	30.8
1	0.237	0.0076	31.18
2	0.249	0.0079	31.52
4	0.494	0.0103	47.96
9	0.834	0.0145	57.52

Table 4. Details of numerical simulations and their extracted powers.

	U_{in} (m/sec)	EI (Pa.m^4)	Extracted power (μW)
Simulation 1	2	0.0015	35
Simulation 2	5	0.008	72
Simulation 3	10	0.02	78

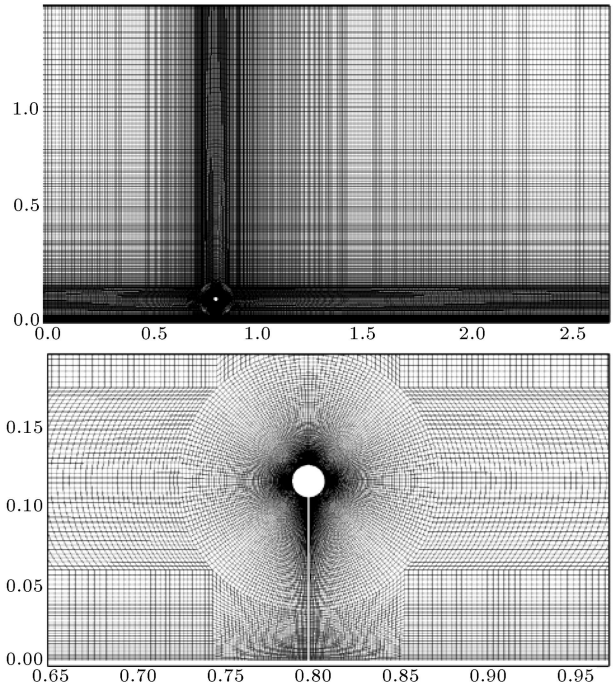

Figure 12. Computational grid for the flexible vertical beam with attached circular cylinder.

tion, the end cylinder is modeled rigidly. Consequently, the flow forces and moments on the cylinder are applied as concentrated ones on the beam tip. Moreover, the displacements of the cylinder nodes are set to the beam tip displacement.

For these simulations, the time history of beam tip displacement and the produced voltage are shown in Figures 13 and 14, respectively.

These figures reveal that the added cylinder intensifies the oscillations of the beam extensively and leads to extracting of remarkable power. Therefore, unlike the sole vertical beam, the new harvester has a good performance in low velocities. Figure 15 displays the deformed shape of beam with its end cylinder for simulation 3 when beam has its maximum deflection.

4. Conclusion

In the present work, the PEH from piezoelectric vertical beams in horizontal fluid flow with different inlet velocities was investigated. It was shown that

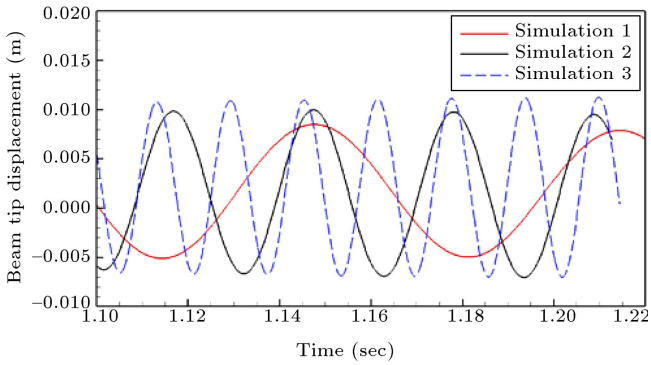

Figure 13. Time history of the vertical pate tip displacement with attached cylinder for $R = 10$ MΩ.

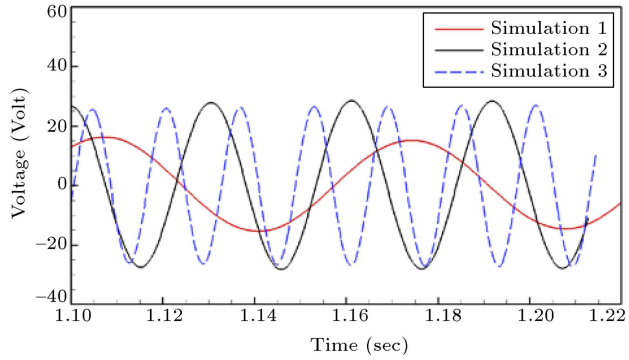

Figure 14. Time history of the produced voltage (Volt) for $R = 10$ MΩ.

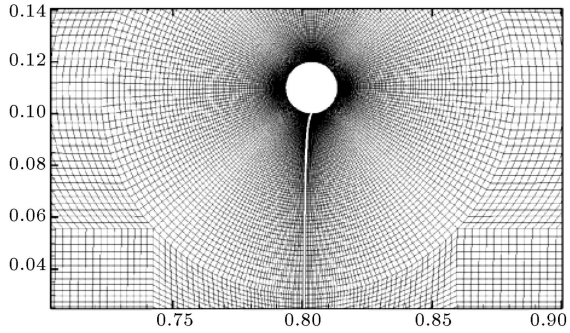

Figure 15. Deformed shape of flexible vertical beam with attached cylinder.

the piezoelectric vertical beams in high-speed horizontal fluid had remarkable vibrations and, therefore, produced considerable electrical power through the piezoelectric effect. However, since in low-speed flows the vibrations were negligible, the extracted power was not considerable. For low-speed flows, the vibrational behavior of the vertical beams could become more effective by attaching an end cylinder to them. It was shown that this shape remarkably intensified the oscillations of the vertical beam and, therefore, the extracted power in low-speed flow. Finally, a piezoelectric energy harvester for aerospace vehicles was introduced. Since in such vehicles, conserving the aerodynamic performance was a crucial rule, a piezoelectric Gurney

flap was used for energy harvesting from fluid flow. By using a Gurney flap, the vibrational energy was converted to the electrical one, while the aerodynamic performance of the vehicle was conserved. It was shown that a piezoelectric Gurney flap attached to the NACA2412 airfoil provided an acceptable value of harvested power.

References

1. Christin, D., Mogre, P.S. and Hollick, M. "Survey on wireless sensor network technologies for industrial automation: The security and quality of service perspectives", *Future Internet*, **2**(2), pp. 96-125 (2010).
2. Jiming, C., Xianghui, C., Peng, C., Yang, X. and Youxian, S. "Distributed collaborative control for industrial automation with wireless sensor and actuator networks", *Industrial Electronics, IEEE Transactions on*, **57**(12), pp. 4219-4230 (2010).
3. Wu, N., Wang, Q. and Xie, X. "Ocean wave energy harvesting with a piezoelectric coupled buoy structure", *Applied Ocean Research*, **50**, pp. 110-118 (2015).
4. Xie, X.D. and Wang, Q. "Energy harvesting from a vehicle suspension system", *Energy*, **86**, pp. 385-392 (2015).
5. Park, G., Rosing, T., Todd, M.D., Farrar, C.R. and Hodgkiss, W. "Energy harvesting for structural health monitoring sensor networks", *Journal of Infrastructure Systems*, **14**(1), pp. 64-79 (2008).
6. JeongGil, K., Chenyang, L., Srivastava, M.B., Stankovic, J.A., Terzis, A. and Welsh, M. "Wireless sensor networks for healthcare", *Proceedings of the IEEE*, **98**(11), pp. 1947-1960 (2010).
7. Ruiz-Garcia, L., Lunadei, L., Barreiro, P. and Robla, I. "A review of wireless sensor technologies and applications in agriculture and food industry: State of the art and current trends", *Sensors*, **9**(6), pp. 4728-4750 (2009).
8. Xie, X.D., Wang, Q. and Wang, S.J. "Energy harvesting from high-rise buildings by a piezoelectric harvester device", *Energy*, **93**, Part 2, pp. 1345-1352 (2015).
9. Xie, X.D., Wu, N., Yuen, K.V. and Wang, Q. "Energy harvesting from high-rise buildings by a piezoelectric coupled cantilever with a proof mass", *International Journal of Engineering Science*, **72**, pp. 98-106 (2013).
10. Liao, W.H., Wang, D.H. and Huang, S.L. "Wireless monitoring of cable tension of cable-stayed bridges using PVDF piezoelectric films", *Journal of Intelligent Material Systems and Structures*, **12**(5), pp. 331-339 (2001).
11. Chalard, L., Helal, D.L., Verbaere, A. and Wellig Zory, J. "Wireless sensor networks devices: overview, issues, state-of-the-art and promising technologies", *ST Journal of Research*, **4**(1), pp. 4-8 (2007).
12. García-Hernández, C.F., Ibarguengoytia-Gonzalez, P.H. and Perez-Diaz, J. "Wireless sensor networks and applications: A survey", *IJCSNS International Journal of Computer Science and Network Security*, **7**(3), pp. 264-273 (2007).
13. Gao, P.X., Song, J., Liu, J. and Wang, Z.L. "Nanowire piezoelectric nanogenerators on plastic substrates as flexible power sources for nanodevices", *Advanced Materials*, **19**(1), pp. 67-72 (2006).
14. Arnold, D.P. "Review of microscale magnetic power generation", *Magnetics, IEEE Transactions on*, **43**(11), pp. 3940-3951 (2007)
15. Beeby, S.P., Torah, R.N., Tudor, M.J., Glynne-Jones, P., O'Donnell, T., Saha, C.R. and Roy, S. "A micro electromagnetic generator for vibration energy harvesting", *Journal of Micromechanics and Microengineering*, **17**(7), pp. 1257-1265 (2007).
16. Glynne-Jones, P., Tudor, M., Beeby, S. and White, N. "An electromagnetic, vibration-powered generator for intelligent sensor systems", *Sensors and Actuators A*, **110**(1-3), pp. 344-349 (2004).
17. Elvin, N.G. and Elvin, A.A. "A general equivalent circuit model for piezoelectric generators", *Journal of Intelligent Material Systems and Structures*, **20**(1), pp. 3-9 (2009).
18. Erturk, A. and Inman, D.J. "An experimentally validated bimorph cantilever model for piezoelectric energy harvesting from base excitations", *Smart Materials and Structures*, **18**(2), p. 025009 (2009).
19. Lu, F., Lee, H.P. and Lim, S.P. "Modeling and analysis of micro piezoelectric power generators for micro-electromechanical-systems applications", *Smart Materials and Structures*, **13**(1), p. 57 (2004).
20. Mitcheson, P.D., Miao, P., Stark, B.H., Yeatman, E.M., Holmes, A.S. and Green, T.C. "MEMS electrostatic micropower generator for low frequency operation", *Sensors and Actuators A: Physical*, **115**(2-3), pp. 523-529 (2004).
21. Nguyen, D.S., Halvorsen, E., Jensen, G.U. and Vogl, A. "Fabrication and characterization of a wideband MEMS energy harvester utilizing nonlinear springs", *Journal of Micromechanics and Microengineering*, **20**(12), p. 125009 (2010).
22. Chiu, Y. and Tseng, V.F.G. "A capacitive vibration-to-electricity energy converter with integrated mechanical switches", *Journal of Micromechanics and Microengineering*, **18**(10), p. 104004 (2008).
23. Jeon, Y.B., Sood, R., Jeong, J.H. and Kim, S.G. "MEMS power generator with transverse mode thin film PZT", *Sensors and Actuators A: Physical*, **122**(1), pp. 16-22 (2005).
24. Choi, W.J., Jeon, Y., Jeong, J.H., Sood, R. and Kim, S.G. "Energy harvesting MEMS device based on thin film piezoelectric cantilevers", *J. Electroceram*, **17**(2-4), pp. 543-548 (2006).
25. Sodano, H.A., Park, G. and Inman, D.J. "Estimation of electric charge output for piezoelectric energy harvesting", *Strain*, **40**(2), pp. 49-58 (2004).

26. Priya, S. "Advances in energy harvesting using low profile piezoelectric transducers", *J. Electroceram*, **19**(1), pp. 167-184 (2007).

27. Dutoit, N.E., Wardle, B.L. and Kim, S.-G. "Design considerations for mems-scale piezoelectric mechanical vibration energy harvesters", *Integrated Ferroelectrics*, **71**(1), pp. 121-160 (2005).

28. Roundy, S. and Wright, P.K. "A piezoelectric vibration based generator for wireless electronics", *Smart Materials and Structures*, **13**(5), p. 1131 (2004).

29. Erturk, A. and Inman, D.J. "Issues in mathematical modeling of piezoelectric energy harvesters", *Smart Materials and Structures*, **17**(6), p. 065016 (2008).

30. Meirovitch, L., *Fundamentals of Vibrations*, McGraw-Hill Higher Education (2002).

31. Erturk, A. and Inman, D.J. "A distributed parameter electromechanical model for cantilevered piezoelectric energy harvesters", *Journal of Vibration and Acoustics*, **130**(4), pp. 041002-041002-15 (2008).

32. Amini, Y., Emdad, H. and Farid, M. "Finite element modeling of functionally graded piezoelectric harvesters", *Composite Structures*, **129**(0), pp. 165-176 (2015).

33. Anton, S.R. and Inman, D.J. "Vibration energy harvesting for unmanned aerial vehicles", In *The 15th International Symposium on: Smart Structures and Materials & Nondestructive Evaluation and Health Monitoring, International Society for Optics and Photonics*, pp. 692824-692824-4 (2008).

34. Allen, J. and Smits, A. "Energy harvesting eel", *Journal of Fluids and Structures*, **15**(3), pp. 629-640 (2001).

35. Taylor, G.W., Burns, J.R., Kammann, S., Powers, W.B. and Welsh, T.R. "The energy harvesting eel: a small subsurface ocean/river power generator", *Oceanic Engineering, IEEE Journal of*, **26**(4), pp. 539-547 (2001).

36. Tang, L., Païdoussis, M.P. and Jiang, J. "Cantilevered flexible plates in axial flow: Energy transfer and the concept of flutter-mill", *Journal of Sound and Vibration*, **326**(1), pp. 263-276 (2009).

37. Akaydın, H.D., Elvin, N. and Andreopoulos, Y. "Energy harvesting from turbulent flows using piezoelectric materials", In *Ankara International Aerospace Conference*, Ankara, Turkey (2009).

38. Akaydin, H.D., Elvin, N. and Andreopoulos, Y. "Energy harvesting from highly unsteady fluid flows using piezoelectric materials", *Journal of Intelligent Material Systems and Structures*, **21**(13), pp. 1263-1278 (2010).

39. Amini, Y., Emdad, H. and Farid, M. "An accurate model for numerical prediction of piezoelectric energy harvesting from fluid structure interaction problems", *Smart Materials and Structures*, **23**(9), p. 095034 (2014).

40. Donea, J., Huerta, A., Ponthot, J.P. and Rodríguez-Ferran, A. "Arbitrary Lagrangian-Eulerian methods", In *Encyclopedia of Computational Mechanics*, John Wiley & Sons, Ltd (2004).

41. Wang, X.S., *Fundamentals of Fluid-Solid Interactions*, Elsevier, Amsterdam, London (2008).

42. Menter, F.R. "Two-equation eddy-viscosity turbulence models for engineering applications", *AIAA Journal*, **32**(8), pp. 1598-1605 (1994).

43. Jasak, H. and Tukovic, Z. "Automatic mesh motion for the unstructured finite volume method", *Transactions of FAMENA*, **30**(2), pp. 1-20 (2006).

44. Jasak, H. and Rusche, H. "Dynamic mesh handling in OpenFOAM", In *Proceeding of the 47th Aerospace Sciences Meeting Including the New Horizons Forum and Aerospace Exposition*, Orlando, FL (2009).

Biographies

Yasser Amini received his BSc, MSc, and PhD degrees in Mechanical Engineering from Shiraz University, Iran, in 2006, 2009, and 2014, respectively. He is currently Assistant Professor in the Department of Mechanical Engineering at Persian Gulf University. His research interests include CFD, mesh-less methods, SPH method, fluid structure interaction, rarefied gas flow dynamics, smart materials, and DSMC method.

Homayoon Emdad received his BS degree in Aerospace Engineering from Washington University, USA, in 1982, and his MS and PhD degrees in the same subject from Kansas University, USA, in 1984 and 1988, respectively. He is currently Associate Professor in the School of Mechanical Engineering at Shiraz University, Iran. His primary research interests are computational fluid dynamics, flow control, fluid structure interaction, meshless methods, multiphase flow, and aerodynamics.

Mehrdad Farid received BS and MS degrees in Mechanical Engineering from Shiraz University, Iran, in 1985 and 1988, respectively, and his PhD degree in the same subject from the University of Calgary, USA, in 1997. He is currently Associate Professor in the School of Mechanical Engineering at Shiraz University, Iran. His primary research interests are computational mechanics, vibration and control analysis, fluid structure interaction, and smart materials.